# Investigations of Low-Temperature Heat Release and Negative Temperature Coefficient Regions of Iso-Paraffinic Kerosene in a Constant Volume Combustion Chamber

Valentin Soloiu<sup>1</sup>, Richard Smith III<sup>1</sup>, Amanda Weaver<sup>1</sup>, Drake Grall<sup>1</sup>, Cesar Carapia<sup>1</sup>, Lily Parker<sup>1</sup>, Marcel Ilie<sup>1</sup>, Mosfequr Rahman<sup>1</sup>, Gustavo Molina<sup>1</sup>

<sup>1</sup>Georgia Southern University, Statesboro, GA

# **ABSTRACT**

Research was conducted to observe the correlation of ignition delay, combustion delay, the negative temperature coefficient region (NTCR), and the low temperature heat release region (LTHR), in a constant volume combustion chamber (CVCC) in relation to blended amounts of isoparaffinic kerosene (IPK) by mass with Jet-A and their derived cetane numbers (DCN). The study utilizes the ASTM standard D7668-14.a in a PAC CID 510 CVCC. The DCN was calculated using the ignition delay and combustion delay measured over 15 combustion events. The fuel blends investigated were 75%Jet-A blended with 25%IPK, 50%Jet-A with 50%IPK, 25%Jet-A with 75%IPK, neat Jet-A, and neat IPK. The ignition delay of neat Jet-A and IPK was found to be 3.26ms and 5.31ms, respectively, and the combustion delay of the fuels were 5.00ms and 17.17 ms, respectively. The ignition delay for 75Jet-A25IPK, 50Jet-A50IPK, 25Jet-A75IPK, fuel blends were found to be 3.5ms, 3.8ms, and 4.2ms, respectively. The combustion delay between the 75Jet-A25IPK, 50Jet-A50IPK, 25Jet-A75IPK, blends are 5.8ms, 7.0ms, and 9.4ms, respectively. The DCNs for 75Jet-A25IPK, 50Jet-A50IPK, 25Jet-A75IPK 43.1, 38.7, and 33.5, respectively. The DCN of the fuel blends compared to neat Jet-A was lower by 10.16% for 75Jet-A25IPK, 19.37% for 50Jet-A50IPK, 30.50% for 25Jet-A75IPK and 46.03% for neat IPK. Blends with larger amounts by mass of IPK resulted in extended ignition and combustion delays. It is concluded that the fuels that have larger amounts of IPK blended within them have extended NTC regions, LTHR regions, and decreased ringing intensity during combustion.

# **NOMENCLATURE**

AHRR Apparent Heat Release Rate

CD Combustion Delay
CI Compression Ignition
CO Carbon Monoxide

CVCC Constant Volume Combustion Chamber

DCN Derived Cetane Number

DI Deionized

DTA Differential Thermal Analysis

Dv(x) Largest Droplet Size of x% of Fuel Spray

EOC End of Combustion FT Fischer-Tropsch HHV Higher Heating Value

HTHR High Temperature Heat Release

ID Ignition Delay

IPK Iso-paraffinic Kerosene LHV Lower Heating Value

LTC Low Temperature Combustion
LTHR Low Temperature Heat Release

NOx Nitrogen Oxides

NTC Negative Temperature Coefficient

NTCR Negative Temperature Coefficient Region

PRR Pressure Rise Rate
RI Ringing Intensity
SMD Sauter Mean Diameter
SOC Start of Combustion
SOI Start of Injection

TAx Temperature at which x% mass of Fuel is Vaporized

TGA Thermogravimetric Analysis UHC Unburnt Hydrocarbons

# INTRODUCTION

The concern of fossil fuel availability continues to grow worldwide as well as the harmful greenhouse gaseous emissions that are produced by the combustion of these fuels. The concern is becoming greater with the emergence of aerospace fuels powering combustion engines utilized for both

commercial and industrial applications [1-2]. Jet-A is a commonly utilized fuel for commercial and military power generation [3]. Conventional fuels, such as Jet-A, are derived from the limited fossil fuel reserves left on earth.

Fischer-Tropsch (FT) synthesis is a process for which produces ultra-clean fuels by converting syngas or biomass into hydrocarbons using various catalysts. The production of these fuels lacks the complexity of their fossil fuel derived alternatives, giving FT fuels greater economic feasibility [4-7]. Iso-paraffinic kerosene (IPK) is a Fischer-Tropsch (FT) derived fuel, whose combustion is known to reduce gaseous emissions and increase thermal efficiency [8-14].

With the usage of emerging advanced combustion technologies, new strategies for mitigating climate change from propulsion and power generation systems can be utilized for reduced emissions. Low temperature combustion techniques have risen into predominance for their ability to reduce  $NO_x$  and soot emissions without the usage of complex/heavy aftertreatment systems [15-17]. Extending the period for which LTHR occurs allows the combustion of the fuel to occur at lower temperatures preventing the formation of  $NO_x$  emissions and lowering the quantity of UHC emissions with the proper fuel being utilized [18-19].

Constant Volume Combustion Chambers are research instruments which can be used to analyze the researched fuels in a controlled environment. This makes analyzing the researched fuels autoignition, temperature rise, pressure rise, and heat release characteristics very accurate. Previous research performed by Soloiu et. al included the study of F-T fuels in a PAC CID 510 CVCC. This study investigated the LTHR, ignition delay, combustion delay, and negative temperature coefficient of neat IPK and ULSD, utilizing a Box-Behnken matrix while changing combustion chamber parameters.

The matrix was utilized to differ the parameters for which injection pressure, pulse width, and wall temperature to determine the effect the parameters had on the LTHR and NTCR regions of neat ULSD and IPK. The research showed that a lower set wall temperature leads to an increased NTCR and LTHR by 10%. Meanwhile, with increased injection pressure and pulse width, the peak combustion pressure for ULSD and IPK was increased by 17.2% and 16.1%, respectively [15].

# THERMO-PHYSICAL PROPERTIES OF THE SELECTED FUELS

Studies of the physical, thermal, and physiochemical properties of the selected fuel blends were conducted to observe how these properties will affect the combustion in a Constant Volume Combustion Chamber (CVCC). These properties are directly related to fuel spray penetration, combustion performance and emissions output [20-23]. All fuel research results in Table 1 were determined using in-house equipment. The POSF batch number for 100 IPK is 7629 and the POSF number for 100 Jet A is 10325.

**Table 1: Properties of All Researched Fuels** 

Tuble 1. 11 operates of this researched 1 dels					
	100 Jet-	75 Jet-	50 Jet-	25 Jet-	100
	A	A	A	A	IPK
		25IPK	50IPK	75IPK	
LHV	41.88	42.31	43.06	43.71	44.25
DCN*	48.0	43.1	38.7	33.3	25.9
Avg. Ignition	3.26	3.49	3.77	4.23	5.31
Delay (ms)					
Avg.	5.01	5.80	6.97	9.47	17.17
Combustion					
Delay (ms)					
Viscosity @	1.32	1.16	1.11	-	1.01
40 °C (cP)					

\*Derived Cetane Number (DCN) obtained using in house equipment. PAC CID 510 governed by ASTM standard D7668-14a. [15,24]

Table 2: Chemical Composition of Jet-A and IPK [25]

Table 2. Chemical Composition of Set-14 and 11 K [25]			
Property	ASTM standard	Jet A	Sasol IPK
POSF number	_	4658	5642
n-Paraffins (wt%)	-	28	2.1
Iso-paraffins (wt%)	=	29	88
Cyclo- paraffins (wt%)	-	20	9
Aromatics (wt%)	Report	20	<0.5
Total sulfur (wt%)	Max 0.3	=	< 0.001

In Table 2 is shown the paraffin and aromatic distribution of neat IPK and Jet-A gathered from previous gas chromatographic investigations [25,29-31]. Paraffins are the primary components in aviation and can be used to predict and explain the physiochemical properties of Jet-A and IPK. Covered in this investigation is the volatility, spray characteristics, heat of combustion, and viscosity [25].

Viscosity affects fuel spray atomization and, in mechanical injection systems, injection timing. An injected fuel that has a large surface area to volume ratio due to a low viscosity and will produce a more complete combustion [23-25]. Fuels with a higher viscosity typically create larger droplets during injection events. Density and viscosity are closely related, and both decrease as temperature increases. Viscosity measurements are done on a Brookfield DV II pro rotational viscometer measured at 2°C increments from 26 °C to 90°C at a spindle speed of 200 rpm. The spindle is submerged in approximately 7.0 mL of the research fuel and the torque being applied to the spindle of the viscometer by the fuel is used to determine viscosity. The viscosity of the fuel is analyzed over a range of temperatures as viscosity changes with temperature.

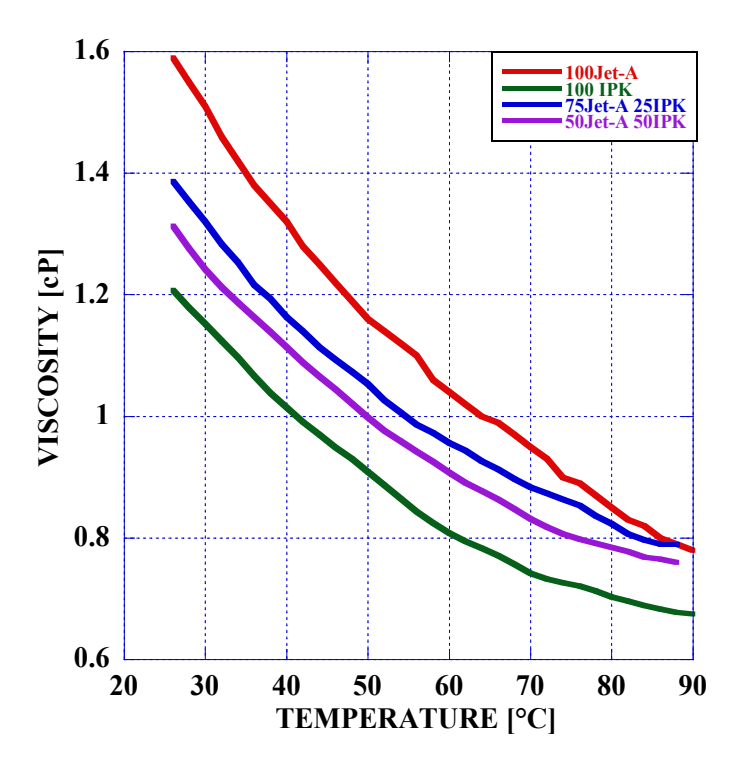


Figure 1: Viscosity Analysis of All Researched Fuels

The graph of the viscosity curve of each fuel is shown in Figure 1. In each of the researched fuels, the viscosity decreases as temperature rises. The viscosity for 100 Jet-A at 40°C was  $1.32~\mathrm{cP}$  while 100 IPK had a much lower viscosity with  $1.01~\mathrm{cP}$  at 40°C. The lower viscosity of IPK as compared to Jet-A can be attributed to its very low aromatic and n-paraffin content. Both components increase both the density and viscosity of the fuel. IPK has an n-paraffin content of 2.1% and an aromatic content of 2.5% as compared to Jet-A which has an n-paraffin content of 2.5% and an aromatic content of 2.5% [25,29].

Each of the fuel blends had a room temperature viscosity between 100 IPK and 100 Jet-A. Viscosities for the blends at 40°C were 1.16 cP for 75Jet-A25IPK, and 1.11 cP for 50Jet-A50IPK.

The Parr 1341 digital constant volume calorimeter was used to determine the lower heating value for each research fuel. Approximately 0.5g of fuel is placed into a crucible and placed in a constant volume chamber. The constant volume chamber is filled with  $O_2$  to 25 atm and placed in 2kg of deionized (DI) water. An Ni alloy fuse wire was strung between two electrodes and an electric current was run through the fuse wire to ignite the fuel in the crucible. On the lid of the jacket is a k-type thermocouple and a stirring impellor. The change in temperature of the DI water is utilized to determine the gross heating value.

100Jet-A and 100IPK have the largest and smallest lower heating values of the research fuels. Neat IPK has the largest lower heating value at 44.25 MJ/kg and neat Jet-A has the smallest lower heating value of 41.88 MJ/kg. A correlation

between the mass percentage of IPK in Jet-A and lower heating value is observed. With an increased mass percentage of IPK present in the blend, the lower heating value of the fuel blend increases. Figure 2 identifies the linearity of the LHV between the neat fuels and their subsequent blends. It is noted that with increasing amounts of IPK in the blends, its linearity remains consistent. The LHV value is averaged across 5 researched calorimetry studies conducted with in-house equipment. The variability between each of the individual studies is less than 5%. The change in the LHV of the fuel is due the H/C ratio of IPK as it is comprised of primarily paraffins of lower carbon number. IPK has larger H/C ratio than that of Jet-A increasing the lower heating value. Additionally, the aromatics present in Jet-A further reduce the lower heating value [29-31].

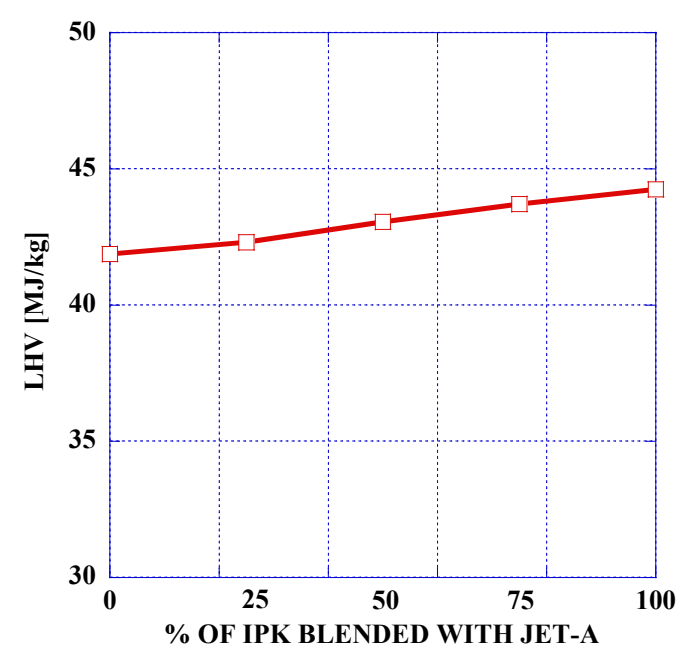


Figure 2: Lower Heating Value of All Researched
Fuels

Fuel Spray characteristics investigation with a Mie scattering He-Ne laser

An investigation was conducted on the spray development/SMD sample distribution of neat Jet-A, neat IPK, and 3 fuel mixtures investigated in this study. The spray distribution research utilized a Malvern Spraytec He-Ne laser apparatus. The He-Ne laser apparatus operates based off Fraunhoffer diffraction and Mie scattering theories to interpret the diffraction of the laser beam emitted through the optical system onto the 32-detector array as shown in Figure 3.

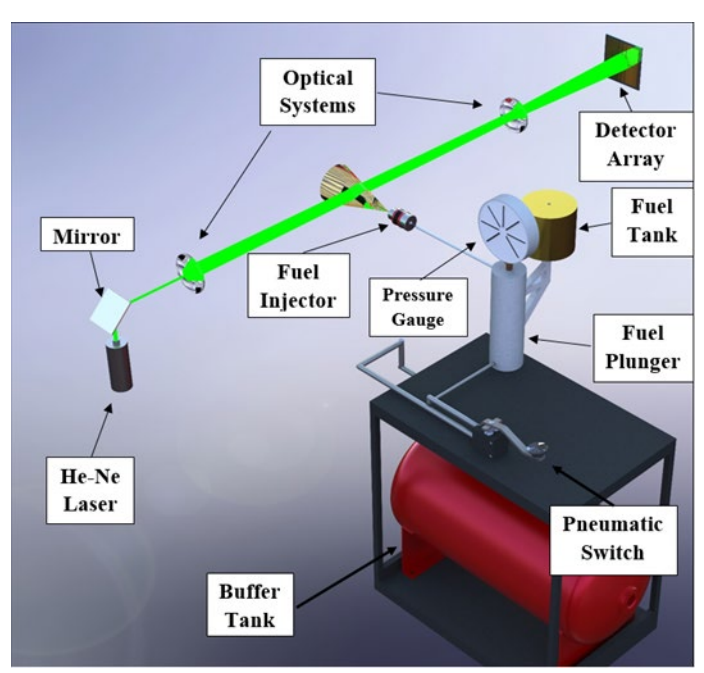


Figure 3: Spraytec Mie Scattering He-Ne laser spray development Analysis Apparatus [32]

Data collection of the selected fuels was conducted at a sampling rate of 10 kHz with an accuracy of  $\pm 0.5 \mu m$  with data acquisition occurring at 1ms after SOI to 5ms after SOI. The fuel was injected by a witness injector with a pressure of 180 bar, 100 mm away from the laser beam.

The average SMD of the researched fuel and volume % distribution for neat Jet-A, neat IPK, 75Jet-A 25IPK (% by mass), 50Jet-A 50IPK, and 25Jet-A 75IPK are shown in Figure 5. It is observed that neat Jet-A's average SMD is greater than all fuels/blends researched for the majority of the injection event, as shown in Figure 4. This is reflected in the volume % distribution as a more of the sprays sample population has a greater SMD than either IPK or the fuel blends. Neat IPK on the other hand, is observed to have an average spray droplet size lesser than all fuels researched with minimal fluctuations occurring possibly due to the lowest viscous fluid's interaction with the injector's nozzle needle towards the end of the injection event. Due to the larger viscosity of Jet-A, Figure 4 suggests that despite the large amounts of IPK present in the fuel blend, 25Jet-A75IPK, there remains a profound effect on average SMD compared to 100 IPK. The small slope between the fuel blends 50Jet-A50IPK and 25Jet-A75IPK, along with the increased slope between the fuel blends 25Jet-A75IPK shown in Figure 4 further solidify the findings.

The influence of IPK % mass used with Jet-A is shown to also effect the % volume distribution of the spray's SMD, with an increase in IPK leading to a greater sample population of the spray droplets occurring at lower SMD However, due to Jet-A's effect on the spray SMD, all fuel blends exhibited a considerable increase in % volume occurring above  $100\ \mu m$ .

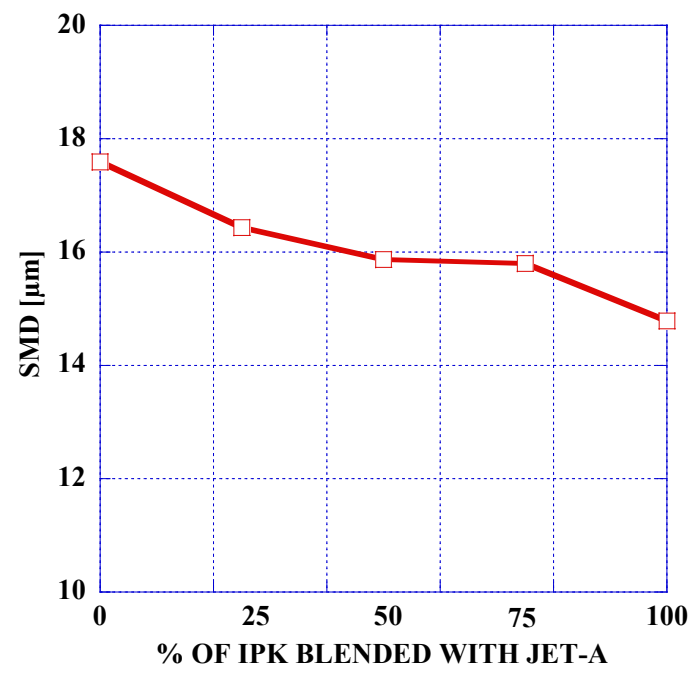


Figure 4: Average SMD for the Researched Fuels

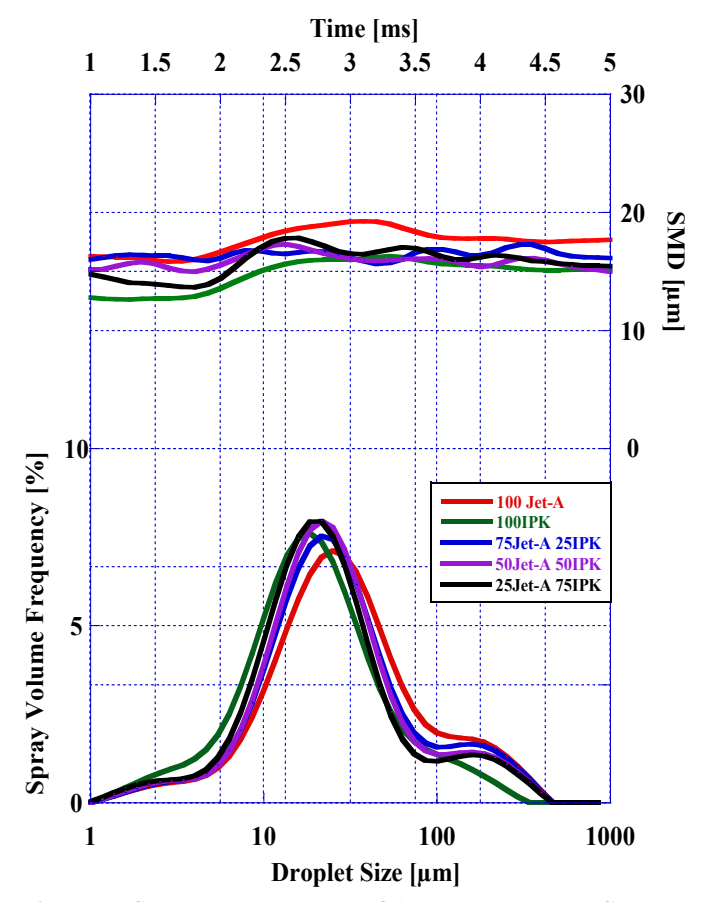


Figure 5: Spray Development of All Research Fuel Sprays IPK's trend to lower the volume % of its spray droplets is further supported with the observations recorded in Table 3,

where 90% of the spray sample population (Dv (90)) for the fuel blends with IPK present kept below 130 um.

The fuel mixture 25Jet-A 75IPK was observed to have the lowest Dv(90) of the blends at  $109.49~\mu m$  which can prove to be advantageous for the combustion of the fuel blend due to the decreased spray SMD allowing for a greater homogenous air/fuel mixture at the site of injection.

The increase in the Sauter Mean Diameter of Jet-A as compared to IPK is due to the increase in the density and viscosity between Jet-A and IPK. This can be attributed to the higher concentration of aromatics, cyclo-paraffins, and n-paraffins in Jet-A [25,29].

**Table 3: Particle Size by Volume** 

Particle Size by Volume	Neat Jet-A	75Jet-A 25IPK	50Jet-A 50IPK	25Jet- A 75IPK	Neat IPK
Dv (10)	9.85	9.22	9.08	8.85	8.27
Dv (50)	30.11	27.08	25.57	25.33	22.96
Dv (90)	133.45	124.67	109.49	112.23	103.34

#### Low Temperature Oxidation and Thermal Stability

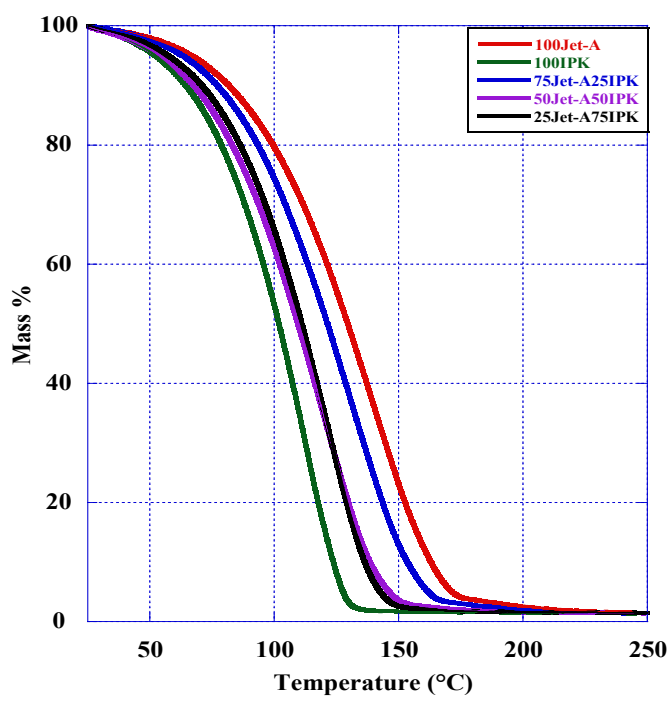


Figure 6: Thermogravimetric Analysis

The Thermogravimetric Analysis (TGA) graph displayed in Figure 6 represents the volatility of the fuel as it vaporizes in relation to temperature. The liquid fuel evaporates into a gaseous state as the temperature in the chamber of the Shimadzu DTG 60, slowly rises to 600°C in increments of 20°C per minute.

This change is measured as a percentage of the starting mass of the research fuel. The temperature at which 10%, 50%,

and 90% of the fuel mass has been vaporized was recorded. These values are denoted as TA10, TA50, and TA90. The results for each of the fuels are shown in Table 4. 100Jet-A is the least volatile of the fuels with a TA90 of 163.00°C. 100IPK is the most volatile fuel with the lowest TA90 of 131.24°C. 25Jet-A75IPK vaporizes with a TA10 of 68°C smaller than that of 50Jet-A50IPK with a TA10 of 71.69°C. 25Jet-A75IPK has a TA90 of 134.92°C, which is also lower than the TA90 of 50Jet-A50IPK of 143.25°C. 75Jet-A25IPK lands above the other two blends with a TA10 of 76.41°C and a TA90 of 153.81°C.

More volatile fuels which vaporize faster are better for combustion as vaporized fuel more easily creates a combustible air-fuel mixture and reduces buildup of fuel in the combustion chamber in areas with poor spray penetration [28]. The increase in the volatility of IPK as compared to Jet-A can be attributed to the high concentration of iso-paraffins of lower carbon number as compared to Jet-A.

These compounds decrease the boiling point and therefore increase the vaporization rate of the research fuel [29,30].

Table 4: Thermogravimetric Analysis (TA(x))

10	Table 4. Thermogravimetric Analysis (TA(x))				
	100Jet-	75Jet-A	50Jet-A	25Jet-A	100IPK
	A	25IPK	50IPK	75IPK	
TA(10)					
(°C)	81.67	76.41	71.69	68.55	71.74
TA(50)					
(°C)	129.53	120.61	113.08	108.25	108.14
TA(90)					
(°C)	163.00	153.81	143.25	134.92	131.24

<sup>\*</sup>The state of the sample is analyzed at 10%, 50%, and 90% mass of fuel vaporized denoted as TA10 TA50 and TA90

A Differential Thermal Analysis (DTA) measures the exothermic and endothermic reactions produced by the fuel as the temperature slowly rises. In the DTA graph in Figure 7, a negative slope is indicative of an endothermic reaction and a positive slope represents an exothermic reaction.

It can be observed that IPK both absorbed more heat than the other fuels and released its energy sooner at around 120°C. Jet-A had a slower energy absorption rate and starts releasing its energy at approximately 135°C.

With the increase in the mass percentage of IPK with Jet-A, the rate of energy absorption and release increases. The changes in energy are measured in  $\mu V/mg$ . Because of the high iso-paraffin content in IPK as compared to Jet-A, the vaporization rate IPK is higher than that of Jet-A.

This means that there is a faster rate of energy absorption for the heat of vaporization [29,31].

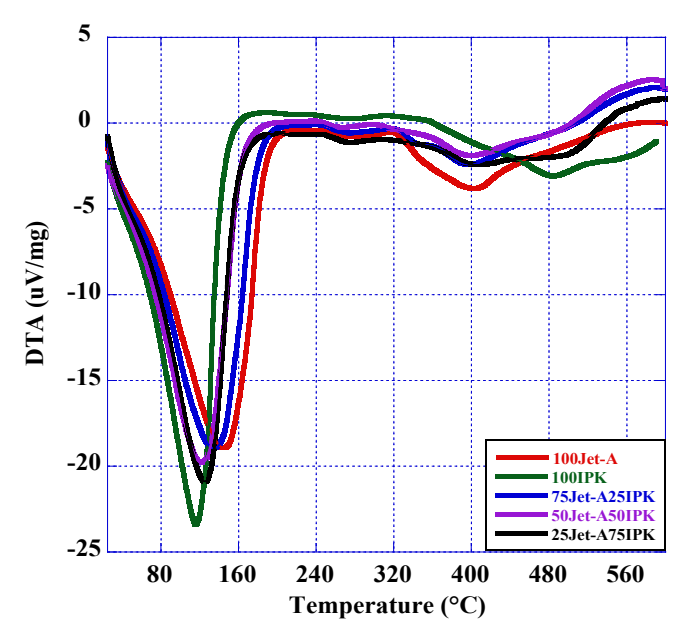


Figure 7: Differential Thermal Analysis

## **CVCC EXPERIMENTAL METHOD**

The PAC CID 510 is a constant volume combustion chamber that analyzes multiple fuel characteristics leading to an average calculation of the research fuel's DCN over 15 combustion cycles.

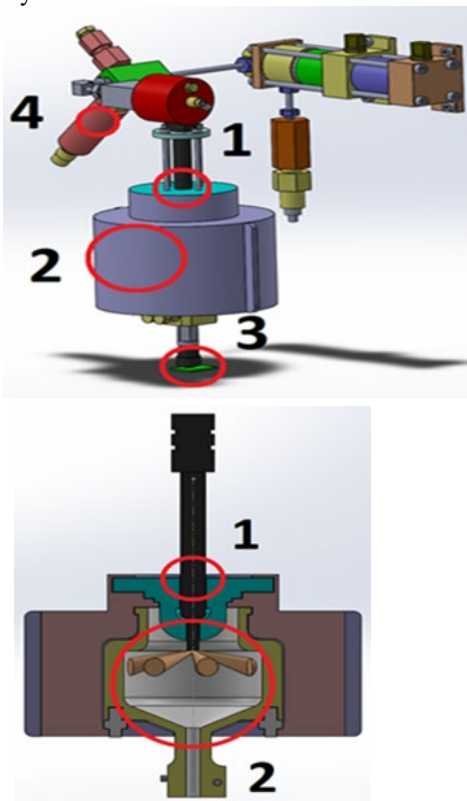


Figure 8: CAD models of the PAC CID 510 [14]

The instrument is comprised of an electronically controlled common rail high-pressure direct injection fuel system (component 1), a uniform heated combustion chamber into which the fuels are injected (component 2), a piezoelectric chamber pressure sensor, (component 3), and an injection pressure sensor (component 4). A CAD model of the PAC CID 510's design and the spray distribution in the combustion chamber is also displayed in Figure 8 below. The DCN, a measurement for the quality of a fuel's autoignition, was determined for each of the research fuels. This measurement is the primary factor for which a fuel is applicable for CI engine use. The DCN value obtained from the CVCC is based off the reactivity of the combustible fuels n-hexadecane and methyl naphthalene, for these combustible fuels have cetane numbers of 100 and 0 respectively [33]. For the neat blends of the research fuels of Jet-A and IPK, the DCNs were measured as 47.95 and 25.88 respectively.

For each analysis, 5 conditioning cycles are performed to prime and stabilize the combustion chamber for the research fuel. Once conditioned, there are 15 injection/combustion cycles. The 15 cycles were analyzed for the average ID and CD of the researched fuel. The DCN then was determined using equation (1). The pressure data recorded for each of the 15 combustion cycles is then post processed to obtain the AHRR of the combustion events.

$$DCN = 13.028 + \left(-\frac{5.3378}{ID}\right) + \left(\frac{300.18}{CD}\right) + \left(-\frac{12567.90}{CD^2}\right) + \left(\frac{3415.32}{CD^3}\right) \quad (1)$$

The ASTM D7668-14a standard is used for all research and is governing the standard operating parameters for DCN determination [24]. The standard parameters include: a wall temperature of 595.5 °C, a fuel injection pressure of 1000 bar, a constant chamber pressure of 20 bar, and an injector pulse width of 2.5 ms, as shown in Table 5.

Table 5: ATSM D7668-14.a Standard Research Parameters

		<u> </u>		
Wall	Fuel	Coolant	Injection	Chamber
Temp.	Injection	Temperature	Pulse	Pressure
	Pressure		Width	
595.5 °C	1000 Bar	50 °C	2.5 ms	20 Bar

The Ignition Delay (ID) in this study is interpreted as the duration from the start of injection, that is at 0 milliseconds on the timeline, to the peak of the LTHR. The start of combustion is defined in this paper as the point where the NTCR ends and HTHR starts. The Combustion Delay (CD) is defined from the start of injection until the time to reach the peak of the HTHR. Both ID and CD are analyzed in milliseconds (ms). EOC is determined as the point where the AHRR curve falls below zero. Ringing events after the initial drop below zero are not considered a component of the combustion event. The cool flame and two stage ignition range for all the research fuels are identified to be between 850K and 950K. This LTHR range is highlighted Figure 9 below. Additionally, the determination of these regions differs depending on each of the research fuels,

100 Jet-A is shown in Figure 9 below with the ID, SOC, CD and EOC regions defined [34-36].

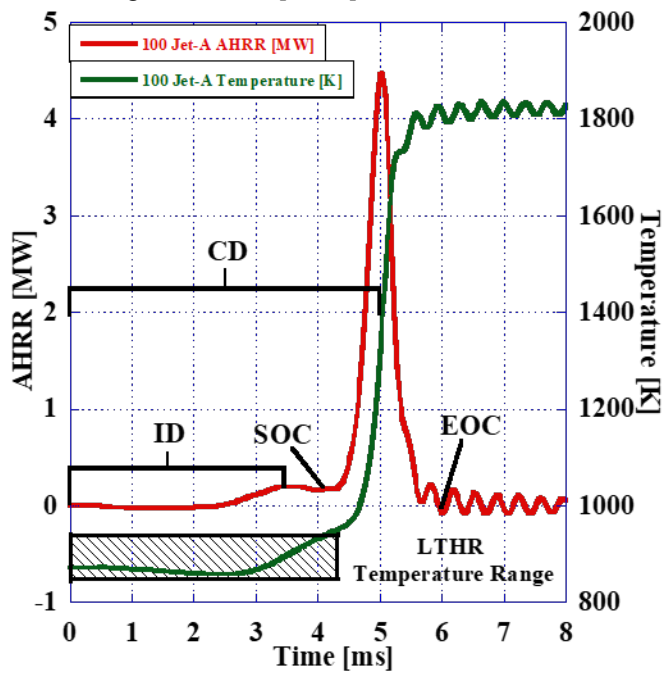


Figure 9: AHRR and Temperature Trace for Jet-A with Denoted ID, CD, SOC, and EOC

#### **DCN Determination Results**

The DCN for the neat fuels Jet-A and IPK were determined to be 47.95 and 25.88, respectively. The ID and CD of Jet-A is 3.03ms and 5.01 ms, respectively, where as IPK's ID and CD is 5.31ms and 17.17ms. The ID of IPK is 1.8 times larger than that of Jet-A, where the CD is 3.5 times larger.

The larger ID and CD of IPK drastically lowers the DCN, as stated above. The autoignition characteristics of IPK may be low, however the energy content of the fuel comparable to Jet-A. The results of the ID, CD, and DCN are presented in Table 6 and Figure 10 below:

Table 6: ID, CD, and DCN Results

Fuel	ID [ms]	CD [ms]	DCN
100Jet-A	3.26	5.01	47.95
75Jet-A 25IPK	3.49	5.8	43.08
50Jet-A 50IPK	3.77	6.97	38.66
25Jet-A 75IPK	4.23	9.47	33.34
100IPK	5.31	17.17	25.88

As shown in Figure 10, with the increasing content of IPK in the fuel blend with Jet-A, the ID and CD increase. These increasing amounts of IPK also decrease the DCN. A line of best fit is added to illustrate the effect of increasing the mass percentage of IPK on a Jet-A base fuel.

The DCN value for each researched blend was heavily influenced by the CD measured. CD influences DCN at an exponential rate as seen in Eq (1), whereas ID only influences

the DCN at a linear rate. The effect of ID is still significant, however, as it identifies the moment at which the peak of LTHR is found. IPK has an extended duration of CD resulting in the sharp decrease in DCN and increased slope of CD shown in Figure 10.

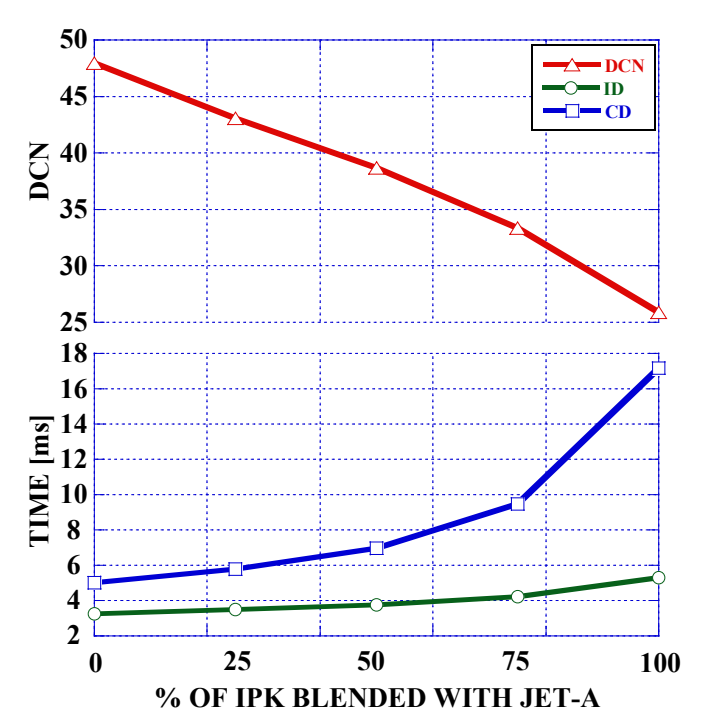


Figure 10: Derived Cetane Number, Ignition Delay, and Combustion Delay for All Fuels

# Combustion Pressure and Mass Fraction Burned

The in-cylinder combustion pressure is measured with the piezoelectric pressure sensor, component 3 in Figure 8. The pressure data collected by this sensor is then utilized for post processing, and the 15 combustion cycles are recorded. The 15 cycles are then averaged to be applied for calculations of the AHRR and combustion chamber average temperature.

The pressure trace for the research fuels are displayed in Figure 11, and the peak pressures are shown in Figure 12. It was observed in the peak pressure trace of Jet-A in Figure 11 that multiple ringing events occurred around the peak pressure. This is opposed to the pressure trace of 100IPK, where there no ringing events occurring after reaching peak pressure. This increase in ringing is influenced by the larger reactivity of 100 Jet-A, as identified by the 54% increase in DCN compared to 100 IPK.

Additionally, the rapid increase in combustion pressure results in a higher magnitude of oscillations occurring after peak pressure, as observed by Soloiu et.al [15].

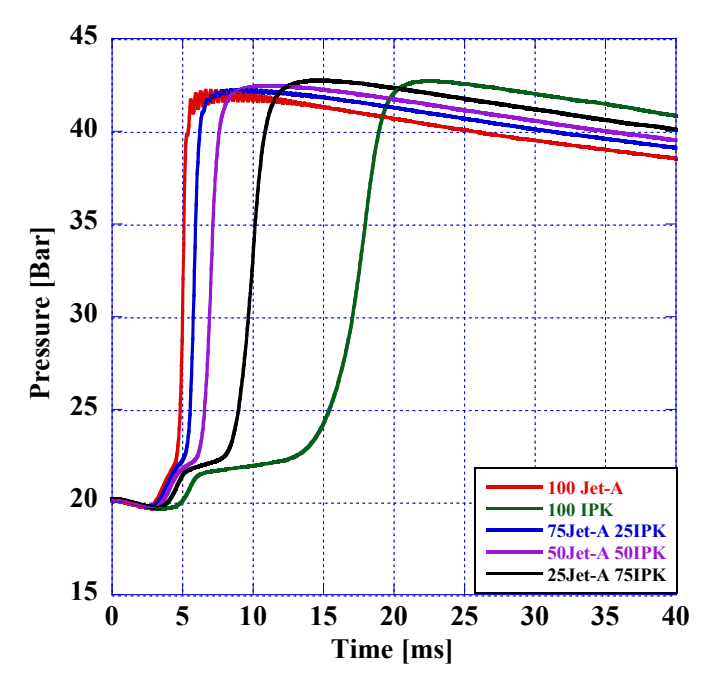


Figure 11: Pressure vs Time for All Research Fuels

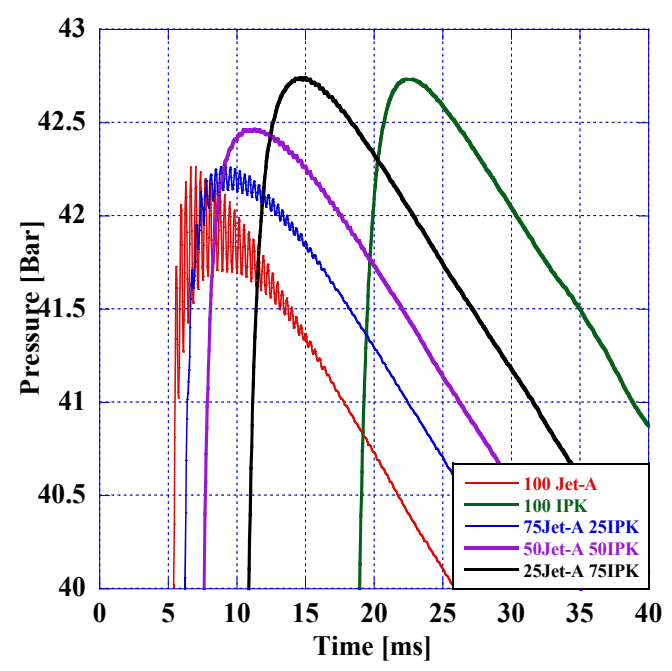


Figure 12: Ringing Measurement for All Researched Fuels

As more IPK is present in the blend, the ringing occurring is reduced. 25Jet-A 75IPK and 100IPK both have practically zero ringing occurring after the peak pressure event. 25Jet-A 75IPK achieved the largest peak pressure across all researched blends with a peak pressure of 42.72 bar, 0.42 bar larger than 100Jet-A and 0.11 bar larger than 100IPK. All peak pressures are shown in Table 6.

**Table 6: Peak Pressures Measured in the CVCC** 

Test Fuel	Peak Pressure (Bar)
100Jet-A	42.26
75Jet-A 25IPK	42.27
50Jet-A 50IPK	42.47
25Jet-A 75IPK	42.74
100IPK	42.73

As noted in Figure 11 and in the AHRR analysis, the fuel blends that possess higher amounts of IPK begin to develop triple stage combustion characteristics. Triple stage combustion characteristics include prolonged stages of LTHR, with an elongated NTCR, that separates the peak HTHR and LTHR. The results for mass fraction burned is identified in Figure 13 below:

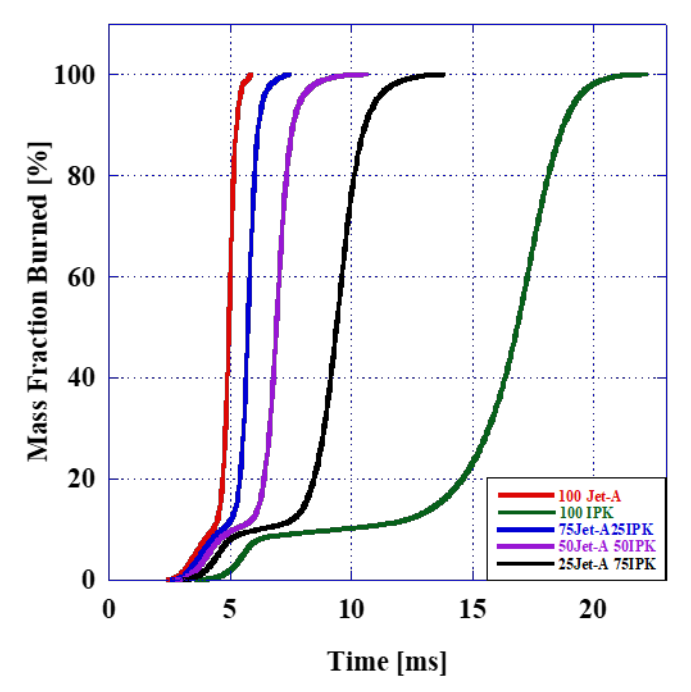


Figure 13: Mass Fraction Burned over Time of the Research Fuels

Nearly the entire mass of 100Jet-A is burned before ignition time of IPK begins. As more by mass amounts of IPK are present in the blend, the period for which the research fuel's burn is extended almost exponentially. This is confirmed by the ID, CD, and DCN results, analysis of the apparent heat release rate provides further insight to into the mass burned results.

### Apparent Heat Release Rate, NTCR, and LTHR Analysis

The Apparent Heat Release Rates (AHRR), are analyzed with Figures 14 and 15. Figure 14 includes the entirety of the AHRR for each fuel. Each fuel mass injected into the combustion chamber has a difference of less than 2% between the researched fuels. Figure 15 is illustrating the LTHR region

of the AHRR for each fuel. These AHRR use a closed system governing equation (Equation 2) in which the heat transfer is neglected (wall maintained at 595.5°C, with no leak through crevices and combustion efficiency is considered 100%). The global specific heat ratio is considered constant, each injection produces a homogeneous mixture, and the data acquisition time step is constant at 0.04 ms throughout the combustion cycle. The global specific heat ratio was given as an overall average through the process [15,34-37]

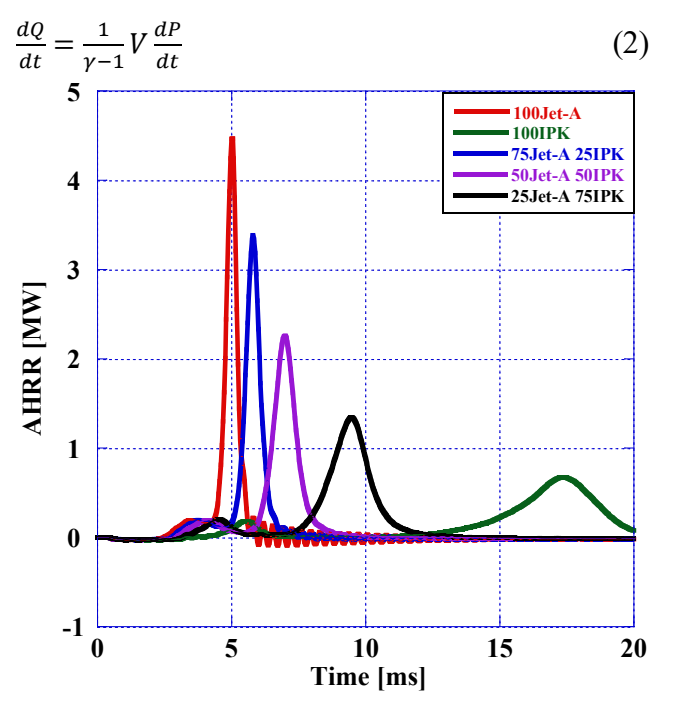


Figure 14: AHRR for All Researched Fuels

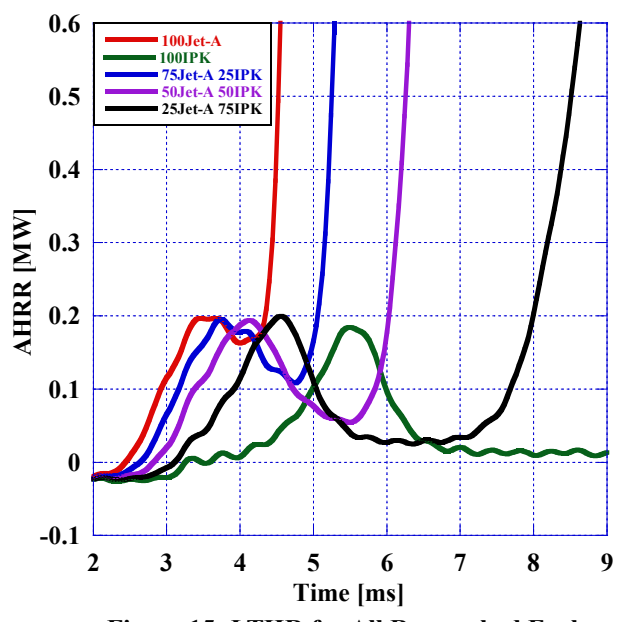


Figure 15: LTHR for All Researched Fuels

100Jet-A has the largest peak AHRR, releasing 4.47 MW during combustion. 100 IPK has the lowest peak AHRR releasing only 0.67 MW at its peak, 85% smaller than that of 100Jet-A. However, 100 IPK possess a unique triple ignition characteristic which includes the dual-peak heat release events with a prolonged NTCR separating the regions. All the blended fuels experience larger NTCR than Jet-A, these regions reduce the HTHR from each of the blends, as shown in Table 7.

Table 7: Peak AHRR/HTHR for All Researched Fuels

Fuel	Peak AHRR [MW]	% Lower Compared to 100 Jet-A
100Jet-A	4.74	N/A
75Jet-A 25IPK	3.39	24.3%
50Jet-A 50IPK	2.26	49.5%
25Jet-A 75IPK	1.24	72.4%
100 IPK	0.67	84.9%

LTHR region is a region for which the research fuels are undergoing periods of slow oxidation and cool flames, as shown in Figure 15. This slow oxidation creates the predominate two stage ignition characteristics occurring in 100IPK and the blends with 50% or more by mass amounts of IPK. Cool flames occur when only a few of the reactants of the fuel oil mixture have reacted and increased in temperature by small amounts [36]. The slow oxidation creates the cool flames that are then quenched, followed by a hot flame that causes a rapid high temperature combustion after the fuel's ignition. The cool flame and two stage ignition range for all the research fuels are identified to be between 850K and 950K [34-36].

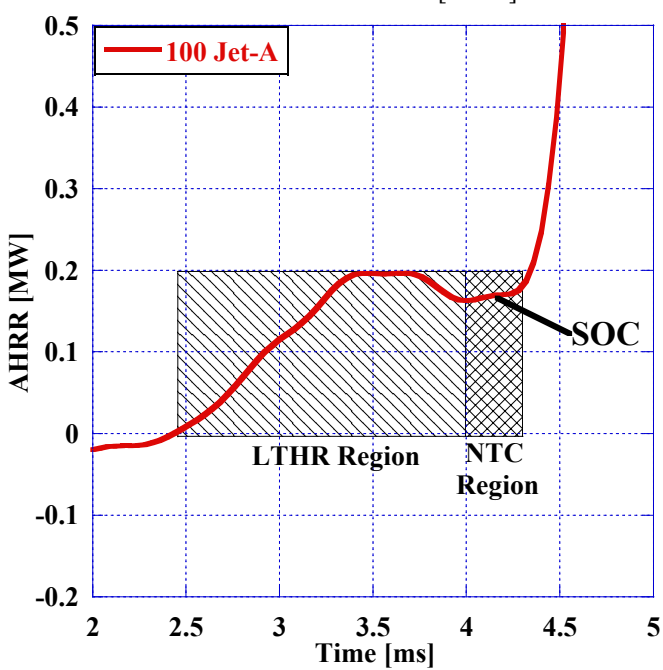


Figure 16: Regions for LTHR and NTC, AHRR of 100Jet-A [15,32]

The LTHR Region encompasses the region on the AHRR where the balance becomes positive. The heat release offsets the heat absorbed by the vaporization of the fuel in spray after the start of injection. The LTHR region extends to beginning of the NTC region where the negative sloping inflection point occurs before the main plateau of NTCR. The NTCR encompasses the plateau after the LTHR before high temperature combustion is established. Once hot temperature combustion has started, the hot flame propagation occurs throughout the HTHR as illustrated in Figure 16 [15,32].

Each of the research fuels' durations within the LTHR, NTC, and HTHR regions are recorded in Table 8.

**Table 8: LTHR Duration of All Researched Fuels** 

Fuel	LTHR Duration [ms]	NTC Duration [ms]	HTHR Duration [ms]
100 Jet-A	1.52	0.28	1.56
75Jet-A 25IPK	1.88	0.34	2.48
50Jet-A 50IPK	2.16	0.76	4.76
25Jet-A 75IPK	2.76	1.64	6.24
100 IPK	3.76	4.00	10.76

Extended durations of LTHR region release more energy and thus reduce the quantity of fuel combusted at higher temperatures during HTHR. Table 9 below identifies how much energy each blend releases during each phase of combustion:

Table 9: Percent Energy Released During Each Combustion Phase

Fuel	LTHR %	NTCR %	HTHR %
100 Jet-A	7.86	2.09	90.05
75Jet-A 25IPK	9.34	1.81	88.85
50Jet-A 50IPK	9.57	1.93	88.50
25Jet-A 75IPK	9.6	2.18	88.22
100 IPK	8.96	2.02	89.02

The blends with 50% and 75% IPK, 50Jet-A 50IPK and 25Jet-A 75IPK, began to exhibit similar triple combustion characteristics as 100 IPK. The extended NTCR occurring after peak LTHR gives the blended fuels these unique characteristics.

During combustion, the blended fuels release more energy during the LTHR and NTCR than the neat Jet-A or neat IPK. It appears that IPK extends the periods for which LTHR and NTCR are occurring allowing the release of more energy during these longer periods.

**Table 10: Cycle Peak Temperatures** 

Tuble 10. Cycle 1	cuit remperatures
Fuel	Peak Temperature [K]
100 Jet-A	1835.44
75Jet-A 25IPK	1835.84
50Jet-A 50IPK	1844.24
25Jet-A 75IPK	1855.25
100 IPK	1850.65

The blends of 50Jet-A 50IPK and 25Jet-A 75IPK also maintain the highest peak pressure and temperature compared to the other researched fuels.

#### CONCLUSIONS

Research was conducted to observe the correlation of ignition delay, combustion delay, the negative temperature coefficient region (NTCR), and the low temperature heat release region (LTHR), in a constant volume combustion chamber (CVCC) in relation to blended amounts of isoparaffinic kerosene (IPK) by mass with Jet-A and their derived cetane numbers (DCN). The thermo-physical characteristics of the fuels researched were evaluated to gain insight on the combustion characteristics observed in the CVCC investigations.

It was found that the lower viscosity of IPK as compared to Jet-A can be attributed to its very low aromatic and n-paraffin content. Meanwhile, neat IPK has the largest lower heating value at 44.25 MJ/kg and neat Jet-A has the smallest lower heating value of 41.88 MJ/kg. A correlation between the mass percentage of IPK in Jet-A and lower heating value, viscosity, and density was observed.

It was found that the IPK amount in the blend, had a significant effect on the spray development and mixture formation as reflected in the Mie scattering spray investigation. It was observed that IPK had reduced the SMD of the spray with its influence greatest at Dv (50) with a reduction of 5  $\mu$ m from 100% Jet-A to 75Jet-A 25IPK.

100 IPK should have more favorable characteristics for autoignition with its smaller droplet size and spray distribution, lower viscosity, and better vaporization than 100 Jet-A. However, due to its chemical composition and very low DCN of about 26, it had the longest ID and CD. The values of the ID and CD of the blends were found to have an inverse correlation with the DCN. For IPK, the DCN decrease of 46% correlates to an increase of ID and CD of 38.6% and 70.8%, respectively, compared to Jet-A. The ID of IPK is 1.8 times larger than that of Jet-A, and the CD is 3.5 times larger. In fact, nearly the entire mass of 100Jet-A is burned before ignition time of IPK.

An attribute of the autoignition quality of IPK is the triple ignition characteristics observed in the AHRR. The extended NTCR located after LTHR and prior to peak HTHR is unique to IPK. This is defined as the triple ignition characteristics: LTHR with a slow oxidation and cool flames followed by quenching during NTCR and finally hot flames propagation and HTHR.

The LTHR duration of IPK is twice as long as that of Jet-A's NTCR while duration is 12 times longer. The triple ignition characteristics of IPK appear to have drastically lower ringing at peak pressure. Ringing was very high for Jet-A and lowered with the increase of IPK in the blend and completely disappearing for the net IPK.

#### **ACKNOWLEDGMENTS**

The Authors would like to acknowledge David Obando Ortegon and Brianna Leckie of Georgia Southern University for their assistance during the paper writing process. Acknowledgment of the contribution of the Air Force Laboratory for suppling the experimental fuels. We would also like to acknowledge Richard Locke, Don Apple, Matthew Tuttle, James Heiler, and Chris Williams from AVL. Charles McGuffy and Michael Rankin from PAC concerning the PAC CID 510, and Joseph Wolfgang from Malvern Lasers. Finally, we would like to acknowledge Richard Smith Jr. P.E. for supporting this endeavor. This paper is based upon work supported by the National Science Foundation Grant No. 1950207.

#### **REFERENCES**

- [1] S. Manigandan, P. Gunasekar, S. Poorchilamban, S. Nithya, J. Devipriya, and G. Vasanthkumar. "Effect of Addition of Hydrogen and TiO2 in Gasoline Engine in Various Exhaust Gas Recirculation Ratio." International Journal of Hydrogen Energy 44, no. 21 (2019): 11205–18.
- [2] C. Gutiérrez-Antonio, F. I. Gómez-Castro, J. A. de Lira-Flores, and S. Hernández, "A review on the production processes of renewable jet fuel," Renewable and Sustainable Energy Reviews, vol. 79, pp. 709–729, 2017.
- [3] J. I. Ryu, K. Kim, K. Min, R. Scarcelli, S. Som, K. S. Kim, J. E. Temme, C.-B. M. Kweon, and T. Lee, "Data-driven chemical kinetic reaction mechanism for F-24 jet fuel ignition," Fuel, vol. 290, p. 119508, 2021.
- [4] N. H. Leibbrandt, A. O. Aboyade, J. H. Knoetze, and J. F. Görgens, "Process efficiency of biofuel production via gasification and Fischer–Tropsch synthesis," Fuel, vol. 109, pp. 484–492, 2013.
- [5] R. G. D. Santos and A. C. Alencar, "Biomass-derived syngas production via gasification process and its catalytic conversion into fuels by Fischer Tropsch synthesis: A review," International Journal of Hydrogen Energy, 2019.
- [6] V. B. Borugadda, G. Kamath, and A. K. Dalai, "Technoeconomic and life-cycle assessment of integrated Fischer-Tropsch process in ethanol industry for bio-diesel and biogasoline production," Energy, vol. 195, p. 116985, 2020.
- [7] T. Damartzis and A. Zabaniotou, "Thermochemical conversion of biomass to second generation biofuels through integrated process design—A review," Renewable and Sust. Energy Reviews, vol. 15, no. 1, pp. 366–378, 2011.

- [8] V. Soloiu, R. Gaubert, J. Moncada, J. Wiley, J. Williams, S. Harp, M. Ilie, G. Molina, and D. Mothershed, "Reactivity controlled compression ignition and low temperature combustion of Fischer-Tropsch Fuel Blended with n-butanol," Renewable Energy, vol. 134, pp. 1173–1189, 2019.
- [9] C. Atkinson, G. Thompson, M. Traver, and N. Clark, "In-Cylinder Combustion Pressure Characteristics of Fischer-Tropsch and Conventional Diesel Fuels in a Heavy Duty CI Engine," SAE Transactions, vol. 108, pp. 813–836, 1999.
- [10] Y. Jiao, R. Liu, Z. Zhang, C. Yang, G. Zhou, S. Dong, and W. Liu, "Comparison of combustion and emission characteristics of a diesel engine fueled with diesel and methanol-Fischer-Tropsch diesel-biodiesel-diesel blends at various altitudes," Fuel, vol. 243, pp. 52–59, 2019.
- [11] S. Jürgens, P. Oßwald, M. Selinsek, P. Piermartini, J. Schwab, P. Pfeifer, U. Bauder, S. Ruoff, B. Rauch, and M. Köhler, "Assessment of combustion properties of non-hydroprocessed Fischer-Tropsch fuels for aviation," Fuel Processing Technology, vol. 193, pp. 232–243, 2019.
- [12] S. S. Gill, A. Tsolakis, K. D. Dearn, and J. Rodríguez-Fernández, "Combustion characteristics and emissions of Fischer–Tropsch diesel fuels in IC engines," Progress in Energy and Combustion Science, vol. 37, no. 4, pp. 503–523, 2011.
- [13] H. Wang and M. A. Oehlschlaeger, "Autoignition studies of conventional and Fischer–Tropsch jet fuels," Fuel, vol. 98, pp. 249–258, 2012.
- [14] V. Soloiu, C. J. Phillips, C. Carapia, A. Knowles, D. Grall, and R. Smith, "Exploratory Investigation of Combustion and NVH Signature of a Drone Jet Engine Fueled with IPK," AIAA Scitech 2021 Forum, 2021.
- [15] V. Soloiu, J. T. Wiley, R. Gaubert, D. Mothershed, C. Carapia, R. C. Smith, J. Williams, M. Ilie, and M. Rahman, "Fischer-Tropsch coal-to-liquid fuel negative temperature coefficient region (NTC) and low-temperature heat release (LTHR) in a constant volume combustion chamber (CVCC)," Energy, vol. 198, p. 117288, 2020.
- [16] M. Waqas, S. Cheng, S. S. Goldsborough, T. Rockstroh, B. Johansson, and C. P. Kolodziej, "An experimental and numerical investigation to characterize the low-temperature heat release in stoichiometric and lean combustion," Proceedings of the Combustion Institute, 2020.
- [17] M. Mehl, W. J. Pitz, M. Sjöberg, and J. E. Dec, "Detailed Kinetic Modeling of Low-Temperature Heat Release for PRF Fuels in an HCCI Engine," SAE Technical Paper Series, 2009.

- [18] D. Carder, R. Ryskamp, M. Besch, and A. Thiruvengadam, "Emissions Control Challenges for Compression Ignition Engines," Procedia IUTAM, vol. 20, pp. 103–111, 2017.
- [19] A. J. Torregrosa, A. Broatch, B. Plá, and L. F. Mónico, "Impact of Fischer–Tropsch and biodiesel fuels on trade-offs between pollutant emissions and combustion noise in diesel engines," Biomass and Bioenergy, vol. 52, pp. 22–33, 2013.
- [20] D. Kang, V. Kalaskar, D. Kim, J. Martz, A. Violi, and A. Boehman, "Experimental study of autoignition characteristics of Jet-A surrogates and their validation in a motored engine and a constant-volume combustion chamber," Fuel, vol. 184, pp. 565–580, 2016.
- [21] W. Jing, W. L. Roberts, and T. Fang, "Spray combustion of Jet-A and diesel fuels in a constant volume combustion chamber," Energy Conversion and Management, vol. 89, pp. 525–540, 2015.
- [22] Y. Park, J. Hwang, C. Bae, K. Kim, J. Lee, and S. Pyo, "Effects of diesel fuel temperature on fuel flow and spray characteristics," Fuel, vol. 162, pp. 1–7, 2015.
- [23] D. Kang, D. Kim, V. Kalaskar, A. Violi, and A. Boehman, "Experimental characterization of jet fuels under engine relevant conditions Part 1: Effect of chemical composition on autoignition of conventional and alternative jet fuels," Fuel, vol. 239, pp. 1388–1404, 2019.
- [24] ASTM D7668-14a, "Standard Test Method for Determination of Derived Cetane Number (DCN) of Diesel Fuel Oils—Ignition Delay and Combustion Delay Using a Constant Volume Combustion Chamber Method," ASTM International, West Conshohocken, PA, 2014, www.astm.org
- [25] Zhang, C., Hui, X., Lin, Y., & Sung, C.-J. (2016). Recent development in studies of alternative jet fuel combustion: Progress, challenges, and opportunities. Renewable and Sustainable Energy Reviews, 54, 120–138. <a href="https://doi.org/10.1016/j.rser.2015.09.056">https://doi.org/10.1016/j.rser.2015.09.056</a>
- [26] J. Hwang, Y. Park, C. Bae, J. Lee, and S. Pyo, "Fuel temperature influence on spray and combustion characteristics in a constant volume combustion chamber (CVCC) under simulated engine operating conditions," Fuel, vol. 160, pp. 424–433, 2015.
- [27] A. Alhikami, C.-E. Yao, and W.-C. Wang, "A study of the spray ignition characteristics of hydro-processed renewable diesel, petroleum diesel, and biodiesel using a constant volume combustion chamber," Combustion and Flame, vol. 223, pp. 55–64, 2021.

- [28] F. K. Tsuji and L. D. Neto, "Influence of Vegetable Oil in the Viscosity of Biodiesel A Review," SAE Technical Paper Series, 2008. doi:10.4271/2008-36-0170.
- [29] \*Elfatih E. Elmalik, Bilal Raza, Samah Warrag, Haider Ramadhan, Ehsan Alborzi, and Nimir O. Elbashir, "Role of Hydrocarbon Building Blocks on Gas-to-Liquid Derived Synthetic Jet Fuel Characteristics," Industrial & Engineering Chemistry Research 2014 53 (5), 1856-1865 DOI: 10.1021/ie402486c
- [30] Moses, C. A. (2008). Comparative Evaluation of Semi-Synthetic Jet Fuels. https://doi.org/10.21813/crcav-2-04a
- [31] Wang, X., Jia, T., Pan, L., Liu, Q., Fang, Y., Zou, J.-J., & Zhang, X. (2020). Review on the Relationship Between Liquid Aerospace Fuel Composition and Their Physicochemical Properties. Transactions of Tianjin University, 27(2), 87–109. https://doi.org/10.1007/s12209-020-00273-5
- [32] V. Soloiu, C. Carapia, R. Smith III, A. Weaver, L. McKinney, D. Mothershed, D. Grall, M. Illie, M. Rahman, "RCCI With High Reactivity S8-ULSD Blend and Low Reactivity N-Butanol," American Society of American Engineers, ICEF2020-3010.
- [33] C. Bae and J. Kim, "Alternative fuels for internal combustion engines," Proceedings of the Combustion Institute, vol. 36, no. 3, pp. 3389–3413, Oct. 2016.
- [34] S. Cheng, D. Kang, A. Fridlyand, S. S. Goldsborough, C. Saggese, S. Wagnon, M. J. McNenly, M. Mehl, W. J. Pitz, and D. Vuilleumier, "Autoignition behavior of gasoline/ethanol blends at engine-relevant conditions," Combustion and Flame, vol. 216, pp. 369–384, 2020.
- [35] S. Cheng, C. Saggese, D. Kang, S. S. Goldsborough, S. W. Wagnon, G. Kukkadapu, K. Zhang, M. Mehl, and W. J. Pitz, "Autoignition and preliminary heat release of gasoline surrogates and their blends with ethanol at engine-relevant conditions: Experiments and comprehensive kinetic modeling," Combustion and Flame, vol. 228, pp. 57–77, 2021.
- [36] Heywood, J. 1988, Internal Combustion Engine Fundamentals, McGraw-Hill, New York.
- [37] A Methodology for Cycle-By-Cycle Transient Heat Release Analysis in a Turbocharged Direct Injection Diesel Engine, 2000.